Experimental Astronomy (2022) 53:1017–1035
https://doi.org/10.1007/s10686-021-09830-9

ORIGINAL ARTICLE

Evaluating the night sky background directly from the signal images detected by the ASTRI telescopes

Antonio Alessio Compagnino[1] · Teresa Mineo[1] · Maria Concetta Maccarone[1] · Osvaldo Catalano[1] · Salvatore Giarrusso[1] · Domenico Impiombato[1]

Received: 23 April 2021 / Accepted: 30 December 2021 / Published online: 23 February 2022

Abstract

ASTRI-Horn is an Imaging Atmospheric Cherenkov Telescope characterized by a dual-mirror optical system with a primary mirror diameter of 4.3 m and a curved focal surface covered by silicon photomultiplier (SiPM) sensors managed by an innovative fast front-end electronics. ASTRI-Horn is installed in Italy at the INAF "M.C. Fracastoro" observing station (Mount Etna, Italy); it is the prototype of nine similar telescopes forming the ASTRI MiniArray that will be installed at the Teide Astronomical Observatory, in Tenerife (Canary Islands, Spain). In the ASTRI-Horn camera, the output signals from SiPMs are AC coupled to the front-end electronics stopping any slow varying signals. However, the random arrival of the night sky background photons produces fast fluctuations in the signal that the electronics is able to detect. The noise generated by this effect is proportional to the level of the diffuse night sky background. In this work, we present the analysis of the background data in ASTRI-Horn observations during the period December 2018–March 2019, using images of triggered showers. We compare the results relative to 2018 December 7-8 and 2019 March 6-7 nights with the contemporary night sky background fluxes measured by UVscope. This is a small auxiliary instrument mounted on the external structure of the ASTRI-Horn telescope and devoted to the night sky background evaluation in the UV band. A strong correlation between the considered data was detected. This correlation can be a diagnostic tool to assure the proper behavior of the ASTRI-Horn camera in view of the ASTRI MiniArray implementation. ASTRI-Horn is also equipped with the *Variance* technique able to sample the level of the pixel signals in absence of showers with an high rate. The method presented in this paper, based on shower images, is a new approach that has never been investigated until now. It does not substitute the *Variance*, that will the baseline for the background

✉ Antonio Alessio Compagnino
antonio.compagnino@inaf.it

[1] INAF, Istituto di Astrofisica Spaziale e Fisica Cosmica di Palermo, via U. La Malfa 153, I-90146 Palermo, Italy

evaluation after exhaustive testings, but it is complementary to it when *Variance* data are available. This is the only one method working very well, that can be applied whenever the standard *Variance* method is not operative.

Keywords ASTRI-Horn · Night sky background · UVscope · Imaging atmospheric cherenkov telescopes

1 Introduction

The most successful detection technique in searching for very high energy (VHE, greater than 100 GeV) cosmic gamma-ray sources is the observation from ground of the Cherenkov light generated by secondary particle showers in the atmosphere [10]. Such a technique is the base of the Imaging Atmospheric Cherenkov Telescopes (IACTs), large optical reflectors which concentrate the Cherenkov light onto a multi-pixel camera. Images of the shower in one or several telescopes are analysed to reconstruct the primary gamma-ray parameters. During the observations, the camera pixels are illuminated by a significant amount of night sky background (NSB) light which largely dominates over the electronic noise. The NSB light depends on environmental and atmospheric conditions of the observational site [4] and is a measure of the background noise from which the Cherenkov signals must be discerned; such an operation is generally performed applying tailored cleaning procedures whose selection cuts are based on the knowledge of the NSB level. In general, the NSB conditions cannot be considered constant during observations. They change more or less rapidly depending on zenithal and azimuthal angles, rotation of the field of view and variations of the environmental and atmospheric conditions. It is therefore a good practice to evaluate the NSB level directly from the observational data. Moreover, the knowledge of the actual NSB rate in each camera pixel, possibly influenced by a star in its field of view, is a tool to judge if a pixel can or not be included in the analysis of the Cherenkov images.

As for all IACTs, the problem to correctly evaluate the NSB level is present in the ASTRI-Horn telescope[1], prototype of nine similar telescopes forming the so-called ASTRI MiniArray (ASTRI MA) that will be installed at the Teide Observatory, Canary Islands. The prototype is named ASTRI-Horn in honor of the italian astronomer Guido Horn D'Arturo, who pioneered the use of segmented primary mirrors in astronomy [3]. ASTRI-Horn, located on Mount Etna, Serra La Nave, Italy, at the INAF "M.C. Fracastoro" observing station (37.7°N, 15.0°E, 1740 m a.s.l.), detected the Crab Nebula above an energy threshold of 3 TeV during the commissioning phase [5]. ASTRI-Horn is equipped with various instrumentation for the monitoring of meteorological and environmental conditions [7]. Among them, the UVscope instrument [6], a photon detector mainly devoted to the measurement of the NSB light in the wavelength range 300-650 nm, is mounted on the external structure of the ASTRI-Horn telescope, co-aligned with its optical axis.

[1] http://www.brera.inaf.it/astri-prototipo/

UVscope evaluates the diffuse NSB level with single count technique [6], while ASTRI-Horn is sensitive to the Poissonian fluctuations produced in its camera pixels at the random arrival of NSB photons. The NSB Poissonian noise measured by ASTRI-Horn is proportional to the diffuse NSB level and therefore can be correlated with the values obtained by UVscope. The outcome can be useful to improve the tuning of the ASTRI-Horn Cherenkov signal analysis (e.g. in the image cleaning procedure) as well as the understanding of the camera limits in view of the ASTRI MA implementation. The ASTRI-Horn camera is also equipped with an algorithm implemented at the Field Programmable Gate Array (FPGA) level, called $Variance$ method [12], for measuring the variance of the NSB fluctuations in each pixel.

Aim of this paper is to present the diffuse NSB analysis performed on real data acquired during the Crab Nebula observation campaigns between December 2018 and March 2019 and the correlation between ASTRI-Horn and UVscope obtained as result. After a brief presentation of both ASTRI-Horn and UVscope, the analysed data set is presented together with the procedures to reduce and analyse ASTRI-Horn and UVscope data. Results and conclusions follow.

2 ASTRI-Horn and UVscope: an overview

A complete description of the ASTRI-Horn telescope and of the UVscope instrument can be found in several contributions and references therein (see 5 and 8 for a comprehensive bibliography on ASTRI-Horn and UVscope, respectively); here we recall their basic features.

2.1 ASTRI-Horn

The ASTRI-Horn telescope (see Fig. 1) is characterized by a Schwarzschild-Couder dual-mirror optical design with a 4.3 m diameter primary mirror segmented in 18 hexagonal panels and a monolithic 1.8 m diameter secondary mirror. The diameter of the circle corresponding to 80% of the encircled energy (D80) of the optical point spread function (PSF) is contained in one camera pixel (0.19° angular size) over all field of view (FoV), as shown by [2]. The telescope mirrors focus on the camera the Cherenkov light emitted during the development of the extensive air showers induced by the interaction of the primary cosmic-rays and VHE gamma rays with the atmosphere.

The ASTRI-Horn camera [1] is characterized by 21 Photon Detection Modules (PDMs) each organized in an array of 8×8 Silicon photomultipliers (SiPM) pixels. These SiPMs are sensitive in the 300-900 nm range with the photo-detection efficiency (PDE) shown in Fig. 2. The total effective FoV subtended by ASTRI-Horn Camera is 7.6°.

The analog PDM output signals in ASTRI-Horn camera are managed by a fast front-end electronics (FEE). The acquisition is based on a peak-detector technique, used for the first time in a Cherenkov camera, that registers the maximum of the shaped pulse height.

Fig. 1 ASTRI-Horn, the dual-mirror Cherenkov telescope installed on Mt.Etna, Italy, at the INAF "M.C. Fracastoro" observing station. On the rigth panel it is visible the small UVscope instrument mounted under the primary mirror structure of the ASTRI-Horn telescope

The read-out electronics is AC-coupled to the detector output and so any slow varying signal is blocked. The camera is then blind to the diffuse NSB or to the light from stars in the FoV. However, considering that sky photons actually arrive with a random Poisson time distribution, the fluctuations generated in the electronic signal, that are proportional to the flux, are detected as noise. The background in the ASTRI-Horn camera is then characterised by signals distributed with fluctuations around the zero level (pedestal). The standard deviation of these signals (hereafter signal RMS) is mainly due to reception fluctuations, being both the intrinsic electronic noise and the SiPM dark current much lower than those.

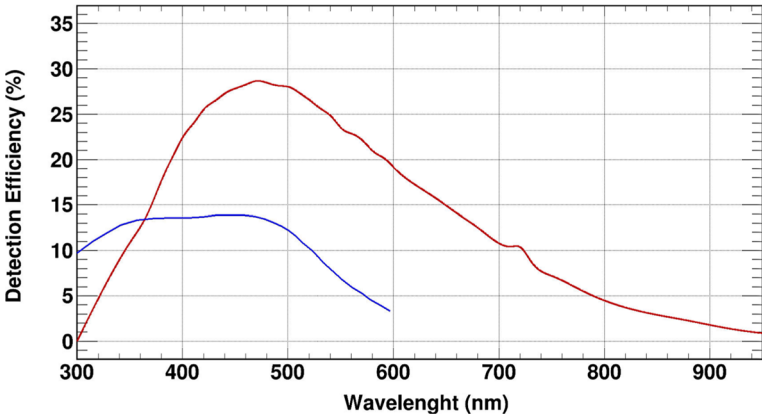

Fig. 2 PDE of the ASTRI-Horn SiPM as a function of the wavelength(red curve).For a comparison the QE of UVscope is shown in blue

The *Variance* algorithm implemented in the FPGA continuously samples the signals of each pixel at the not occurrence of PDM triggers and accumulates the sum of their values and their squares. Whenever the *Variance* is not present, the same information can be obtained with lower statistical significance from images relative to Cherenkov events. In any case, *Variance* data have the high statistical significance (0.4%), being sampled 2^{16} times per seconds. [1, 12, 13].

2.2 UVscope

The UVscope instrument [8] is a light detector developed at INAF/IASF-Palermo and it is mainly devoted to the measurements of the NSB light and atmosphere transparency in the wavelength band 300-650 nm. It is working in single photon counting mode that keeps negligible the electronic noise. UVscope basically consists of:

- a photon detector with its front-end and data acquisition electronics units;
- a disk emulator interface card for computer connection;
- a pinhole collimator to regulate the angular aperture of the detector and to protect its sensitive area against stray light;
- a quartz window, 99% UV transparent and anti-reflecting coated, to protect the sensor against unexpected environmental critical conditions during the data taking;
- a motorized diaphragm to open/close the entrance pupil during night/day;
- an air-ventilation system and the power unit.

For a complete protection against undesired shutter failures during data taking and/or environmental critical conditions, a removable plastic cup is applied at the extreme side of the collimator. The light sensor is a multi-anode photomultiplier tube (MAPMT) with its anodes arranged in a matrix of 8×8 pixels, where each pixel has an effective area of 5.29 mm^2. The Quantum Efficiency (QE) of the MAPMT in shown in Fig. 2, for a comparison with the PDE of the ASTRI SiPMs.

The UVscope instrument is externally mounted under the primary mirror structure of the ASTRI-Horn telescope, as shown in Fig. 1. It acquires data simultaneously with the ASTRI-Horn camera, pointing the same sky region and without any interference with the main telescope. To relate the UVscope measurements as much as possible with the central zone of the ASTRI-Horn camera, a collimator equipped with a 2 mm × 2 mm entrance pupil has been used. The distance between pupil and photocathode has been settled at 238.1 mm so to achieve an angular aperture of UVscope pixel of 0.55°. Under these geometrical conditions, the UVscope field of view covers the central area of about 3×3 PDMs of the ASTRI-Horn camera, being the aperture of each UVscope pixel equal to about 3×3 pixels of the ASTRI-Horn camera (0.19° angular pixel size), as schematized in Fig. 3. The misalignment between UVscope and ASTRI-Horn, verified with pointings on several known stars (i.e. Eta Herculis, Beta Leonis and Zeta Tauri), is $\simeq$0.3° [8]. The effects of this misalignment in the comparison between ASTRI-Horn and UVscope are negligible with respect to the ones due the different working ranges.

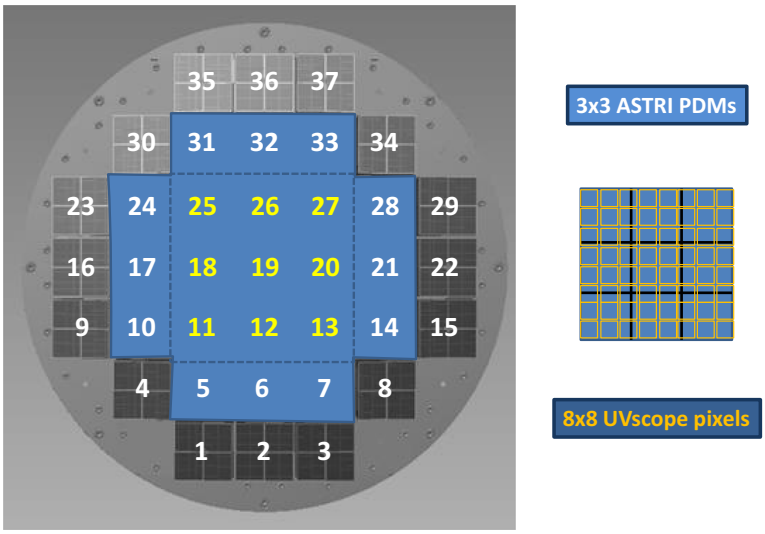

Fig. 3 The ASTRI-Horn focal surface is shown on the left and UVscope pixels (in yellow) superimposed to ASTRI-Horn PDMs with the relative dimensional correspondence on the right. Numbers on the ASTRI-Horn camera code the single PDMs, with the yellow ones roughly identifying the FoV common to UVscope

3 The data set

In the data used in this paper for the diffuse NSB evaluation, a selection was applied to avoid periods affected by technical problems as instability in the PDM signals or fluctuation of the trigger rate as reported in the observation logbook. Moreover, intervals with bad atmospheric conditions (high humidity, low external temperature, cloudiness), as measured by the on-site weather station, were not considered as well as the rare periods when UVscope data were not available. These selections restrict the sample to ∼50% of the available observing nights. The analyzed ASTRI-Horn acquisitions, identified by their run ID number, are listed in Table 1, together with the starting time, exposure, number of acquired events and pointing direction. They are all relative to the same trigger threshold.

It has to be noted that, during the observation period of the telescope commissioning here analyzed, some problems in the ASTRI-Horn optics system were present. In brief, three panels out 18 of the primary mirror were not properly aligned: one of them was covered because not adjustable through the active mirror control, while the other two were found to be misaligned by $\sim 1^\circ$ as detected with a dedicated analysis based on the $Variance$ method [12]. In addition, the secondary mirror experienced a degradation of the reflectivity because of a strong eruption of the Etna volcano on February 2019 and all the following observations were affected by loss of about 25% of the optical throughput respect to the December one [9].

The front-end electronics of the ASTRI-Horn camera is based on two separate chains that allow for high- and low-gain (HG and LG) amplification. During the period here examined, both HG and LG chains were active in case of calibration

Table 1 Observation log of ASTRI-Horn data used in this paper

Run ID	UTC Starting Date (y/m/d h:m:s)	Exposure (s)	N. of events	Pointing RA(deg) Dec(deg)
1429	2018/12/05 20:57:37	2094	31755	46.13, 22.01 (Crab Off)
1430	2018/12/05 21:54:40	909	29808	Fixed AltAzi*
1431	2018/12/05 22:22:29	3573	133190	83.63, 22.01 (Crab)
1432	2018/12/05 23:30:12	3790	450000	83.63, 22.01 (Crab)
1433	2018/12/06 01:27:41	7638	198341	121.13, 22.01 (Crab Off)
1434	2018/12/06 03:36:06	4499	142610	Fixed AltAzi*
1453	2018/12/07 20:06:11	6016	348442	46.13, 22.01 (Crab Off)
1454	2018/12/07 22:09:16	4377	226651	83.63, 22.01 (Crab)
1455	2018/12/07 23:30:08	6243	412451	83.63, 22.01 (Crab)
1456	2018/12/08 01:25:40	8478	237318	121.13, 22.01 (Crab Off)
1457	2018/12/08 03:50:20	3509	126295	Fixed AltAzi*
1464	2018/12/08 20:30:37	2251	97257	46.13, 22.01 (Crab Off)
1465	2018/12/08 21:17:34	9624	430245	83.63, 22.01 (Crab)
1466	2018/12/09 00:07:25	3161	251442	83.63, 22.01 (Crab)
1467	2018/12/09 01:09:44	8959	243713	121.13, 22.01 (Crab Off)
1468	2018/12/09 03:40:11	1237	33168	Fixed AltAzi*
1472	2018/12/09 19:55:03	4958	185142	46.13, 22.01 (Crab Off)
1473	2018/12/09 21:28:40	5549	266294	83.63, 22.01 (Crab)
1486	2018/12/11 23:02:02	1627	100948	83.63, 22.01 (Crab)
1487	2018/12/11 23:31:48	4800	259447	83.63, 22.01 (Crab)
1488	2018/12/12 01:01:45	4928	297577	121.13, 22.01 (Crab Off)
1489	2018/12/12 03:02:43	1744	73285	121.13, 22.01 (Crab Off)
1490	2018/12/12 03:34:02	2537	125218	Fixed AltAzi*
1670	2019/03/06 18:08:27	628	8191	165.46 , 56.38 (Merak)
1671	2019/03/06 18:21:51	126	2412	84.41, 21.14 (Zeta Tauri)
1672	2019/03/06 18:25:56	5935	296073	83.63, 22.01 (Crab)
1673	2019/03/06 20:06:58	183	3272	84.41, 21.14 (Zeta Tauri)
1674	2019/03/06 20:13:37	13812	152393	143.63, 22.01(Crab Off)

*Azi= 180° Elev. = 70°

mode (closed lids) but the HG chain was not operative in sky observation mode (open lids); then we considered only LG data for our scientific analysis. On March 2019 the HG chain was fully activated, but only one pointing, to zenith, was available for our purposes and we used these data (Run ID 1785, March 25 2019) to verify the consistency of the results from HG and LG chains.

UVscope data were acquired each night, simultaneously with the ASTRI-Horn camera; only during two short periods of December 2018 (the beginning of the 7-8 night and second part of the 9-10 night) the acquisition was not performed due to an unexpected switch-off of the instrument.

Last but not least, all ASTRI-Horn and UVscope data have been analysed only if in dark-night regime, with the Sun and the Moon at least 18° below the horizon.

4 ASTRI-Horn data reduction and analysis

The $Variance$ method that is the baseline to compute the NSB statistical variance for each pixel [12] was not used in this analysis because the relative data were not available in December due to a technical problem and, for uniformity purposes, we decided not to use it either in March.

The analysis presented in this paper is based on the images of triggered showers as detected by the ASTRI-Horn camera.

This NSB variance was named $PHDVAR$ to distinguish it from the $Variance$ obtained by the electronics. It was computed with the simple relation $PHDVAR$ equal to the square of the signal RMS around the pedestal. In any case, we checked that, whenever $Variance$ data are available, the two values are equivalent within a systematic error of 1%

As signals are expressed in term of ADC counts per pixel, the first step to be performed is their calibration and conversion to photo-electrons ($p.e.$). Moreover, to evaluate the **PHDVAR** values, pixels including shower signals must be identified and excluded. In this section, the procedures to calibrate, identify and analyse background data are described.

4.1 Data Calibration

The analog signals coming from the camera electronics, digitized through external ADC devices, are converted to $p.e.$ according to the following relation:

$$p.e. = \frac{ADCcounts - Pedestal}{Gain} \tag{1}$$

where $Gain$ and $Pedestal$ are determined from measurements performed by the ASTRI-Horn camera with closed lids and taking into account some reference values previously obtained in laboratory [1].

To evaluate the pixel gains of the ASTRI-Horn camera, we made use of the fiber optical calibration (FOC) system inner to the camera [1, 11]. The FOC blue LED was pulsed at a constant rate of 1 kHz producing an average intensity of a few $p.e.$ per pixel. The procedure for the gain correction is based on the comparison of the mean distance, in ADC counts, between two consecutive peaks of the pulse height distributions produced by the FOC ($p.e._{eq}$) with the value ($p.e._{ref}$) obtained in laboratory with the same method applying a reference gain G_{ref}:

$$G_{FOC} = \frac{p.e._{eq}}{p.e._{ref}} G_{ref} \tag{2}$$

Table 2 Log of FOC data used in the analysis. For these runs HG data are considered

Run ID	Starting Date (year/month/day h:m:s)	Exposure (s)	Number of events
1394	2018/12/02 20:01:09	60	60065
1763	2019/03/23 20:01:21	120	120123

where G_{FOC} is the gain, pixel by pixel in the FOC runs.

Two different calibration acquisitions were performed, one for each main period of scientific observations, as schematized in Table 2. Specifically, run ID 1394 has been used to calibrate December 2018 events, while run ID 1763 has been used for February and March 2019 events.

To compute the $p.e._{eq}$ for each pixel, the pulse height distributions obtained in the HG chain were accumulated and fitted with a multi-Gaussian function, averaging then the measured distance between peaks.

The LG gain was obtained applying the constant ratio between the two electronics chains, as measured in laboratory [1].

The other calibration parameter, the LG pedestal, is obtained from events acquired with the camera lids closed where, in absence of light, only one peak is detected. We accumulated the distributions relative to each single pixel of the two observation runs listed in Table 3 and fitted them with a Gaussian function where the centroid gives the pedestal value.

4.2 Data Analysis

To compute the PHDVARs, we considered only the nine central PDMs (11, 12, 13, 18, 19, 20, 25, 26, 27 in Fig. 3) that match the UVscope FoV. In addition, coherently with the procedure adopted for UVscope data, the ASTRI-Horn camera pixels corresponding to the outer UVscope frame are excluded from the final computation (see Section 5). This reduces the useful pixel number from 576 (64 pixels$\times$9 PDMs) to 324 pixels.

Background pixels in ASTRI-Horn images were identified applying a double cut cleaning procedure similar but complementary to the one used for the selection of Cherenkov shower images, that allows us to discard all the fast signals (shower and muons) and to collect all the slow varying signal (diffuse NSB and stars). This procedure considers background pixels the ones that have a signal lower than a first

Table 3 Log of the observations with camera lids closed. For these runs, LG data are considered

Run ID	Starting Date (year/month/day h:m:s)	Exposure (s)	Number of events
1380	2018/12/01 20:59:18	1760	15305
1616	2019/02/28 12:37:02	9929	50000

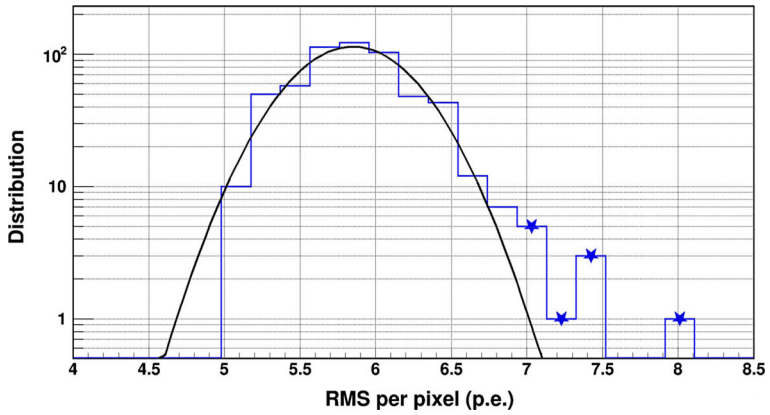

Fig. 4 Distribution of the signal RMS measured in the camera pixels of the nine central PDMs for 5000 events of the run 1453. The black curve represents the Gaussian fit of the distribution. All signal RMS values higher than 3 times the σ of the Gaussian (marked with stars) are not considered as due to background and pixels with these signal RMS are excluded from the analysis (for a total of 9 pixels in this example)

threshold $S1$, or, if higher than $S1$, without any neighbouring pixels with a signal higher than the second threshold $S2$. We adopted the values $S1$= 6 *p.e.* and $S2$=12 *p.e.* used by [9] to identify muon signals, that is also suitable to discard the showers being lower than the thresholds adopted for the analysis of Crab Nebula events [5].

From the $Variance$ data, we know that ASTRI-Horn camera is able to detect stars with an increase of the signal RMS [1]. The evaluation of the background then requires that pixels illuminated by stars must be excluded. The computation of the signal RMS averaged over 5000 events, corresponding to an exposure of ∼2 minutes, follows the two steps listed below:

1. *identification of the pixels illuminated by stars*: for each pixel of the nine central PDMs, we computed the signal RMS of the $p.e$ detected over 5000 events and accumulated the relative distribution; one example of this distribution is shown in Fig. 4. We then modeled the distribution with a Gaussian whose parameters (centroid and σ) were obtained with a fitting procedure (black curve in Fig. 4). We considered as good pixels, i.e. not including stars, the ones whose signal RMS is lower than 3 σ from the average.
2. *evaluation of the average* **RMS**: we computed a single $p.e.$ distribution for the 5000 events and all good pixels (signal RMS lower than 3 σ and lying in the central camera region of size 18×18 pixels). It takes into account the statistics of the distribution as well as the systematic in the pixel gain calibration. We fitted the central part of this distribution with a Gaussian whose sigma is the signal RMS we correlate with the diffuse NSB flux as obtained by the UVscope data. Errors on the best-fit signal RMS values are relative to 68% confidence level. The curve obtained for one of the 5000 bunches in the file ID 1453 is plotted in Fig. 5 as example.

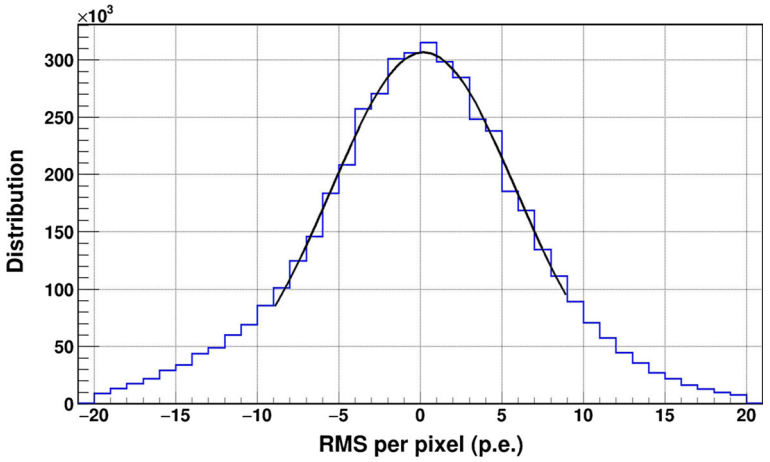

Fig. 5 Distribution of the *p.e.* detected in the 18×18 camera pixels of the nine central PDMs used in the analysis for 5000 events of the run 1453 (blue curve). The black curve is the Gaussian fit of the central region

To cross-check the validity of this procedure, we used March observations when contemporary $Variance$ data were also available. We were able to reproduce with our method the $Variance$ values in each image.

Moreover, using the run ID 1785 where both HG and LG chain are present, we verified that the signal RMS computed from each of the two chains were perfectly coherent.

5 UVscope data reduction and analysis

The data acquired by UVscope are registered, pixel by pixel, as number of counts in a pre-selected integration time (1 s). The conversion from counts to physical units is related to several features (geometrical factor, dark counts, average efficiency, gain uniformity) that characterize the sensor and its configuration, as widely detailed in [8] and briefly reported in the following. The geometrical factor corresponds to about $1.225\ \mathrm{mm}^2 \times \mathrm{deg}^2$; the dark counts has negligible values (0.7 counts/second per pixel) and the mean value of the global efficiency of the entire detection unit (comprehensive of collecting, trigger, quantum efficiencies and quartz windows) results in 11.61%. The gain uniformity map, pixel by pixel, was derived from periodic "flat field" acquisitions obtained by putting a fluorescent paper in the inner part of the collimator cup so to uniformly illuminate the UVscope sensor. For the diffuse NSB evaluation, the 28 pixels of the MAPMT external frame, whose contents are influenced by effects on the edges, are excluded from the analysis. Moreover, the image of a bright star appears in UVscope in maximum 4 pixels (if the star is located across more pixels); such pixels are also excluded from the analysis. The remaining 32 pixels will form the hereafter called "useful mask". The "useful mask" is dynamically

identified, acquisition by acquisition, cutting the 28 pixels along the external perimeter and the first 4 pixels with the highest content as detected in the inner 6×6 pixels region.

In brief, to evaluate the mean flux of the diffuse NSB as a function of time, $< NSB > (t)$, the UVscope data, pixel by pixel, are cleaned of dark counts (albeit very low), normalized to the gain uniformity map of its sensor unit, scaled for the global efficiency of the detection unit itself and, after the selection of pixels in the "useful mask", used for the evaluation of:

$$< NSB > (t) = \frac{CTS^*(t) \cdot 10^{-3}}{GF_{pixel} \cdot < \varepsilon_{total} >} \qquad \left[\frac{photons}{m^2 \cdot ns \cdot sr}\right] \tag{3}$$

with:

$$CTS^*(t) = \frac{1}{Npix} \sum_{k=1}^{Npix} \frac{CTS(k,t) - < dark(T(t)) >}{equ(k)} \qquad \left[\frac{counts}{second}\right] \tag{4}$$

where $< \varepsilon_{total} >$ is the average value of global efficiency and GF_{pixel} the geometric factor of the pixels, k indicates each of the N_{pix} forming the useful mask, CTS_k are the counts in the pixel k at time t, $< dark(T(t)) >$ is the average value of the dark counts in each pixel at temperature T in the time t and $equ(k)$ is the element of the sensor gain equalization map for k pixel in the period in question.

6 Results

We performed the analysis on all data set presented in Table 1, however, we found that only two nights (7-8 December 2018 and 6-7 March 2019) were suitable for the UVscope correlation study, as explained in detail in Section 7.1. All the **PHDVAR** values obtained by the fit of the $p.e.$ distribution, correspondent to the central region (18×18 pixels) of ASTRI-Horn camera and averaged over 5000 events, were compared and correlated with the NSB flux measured by UVscope. The integration time correspondent to the 5000 events depends on the trigger rate of the camera and is on average ∼ 2 minutes. This section presents the obtained results.

6.1 NSB temporal evolution

The temporal evolution of the $PHDVAR$ was computed for the two selected nights and compared with the flux measured by UVscope as shown in Fig. 6 where the light curves relative to the night 2018 December 7–8 and 2019 March 6–7 are displayed in the upper and lower plots, respectively. In each plot, we report the $PHDVAR$ data (top panels) measured by ASTRI-Horn every ∼2 minutes and of the NSB flux measured by UVscope every second (bottom panels) since the beginning of the observation. We note that there is an overall agreement between the two instrument measurements, but also several discrepancies, some of which cannot be easily explained.

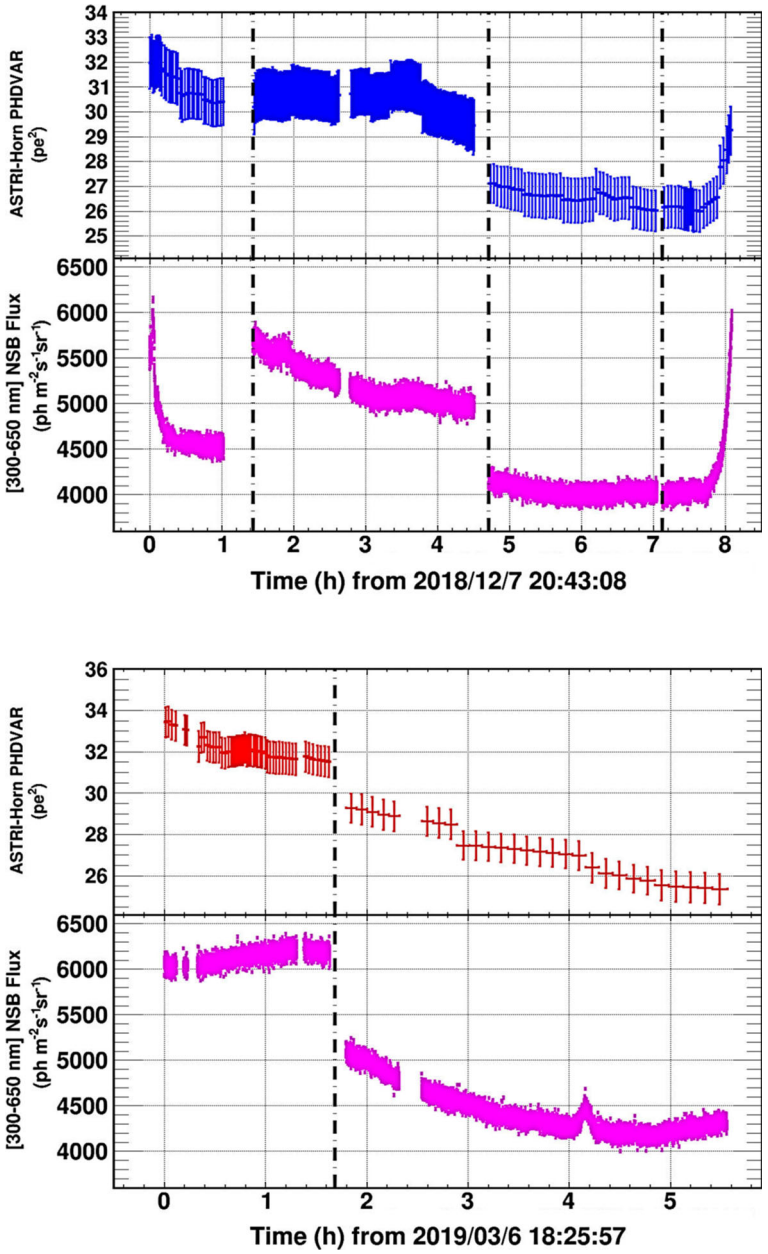

Fig. 6 Temporal evolution of the $PHDVAR$s measured by ASTRI-Horn (top panels) and the NSB fluxes measured by UVscope every second (bottom panels) relative to the observing night 2018 December 7–8 (upper plot) and 2019 March 6-7 (lower plot). The vertical dashed lines indicate variations of the telescope pointings

In particular, it is evident that the **PHDVAR** values measured by ASTRI-Horn follow the jumps in the NSB flux detected when the telescope moves to different observing directions (see vertical dashed lines in the plots) because of the on-off pointing procedure applied during the Crab Nebula observation. ASTRI-Horn **PHDVAR** do not vary significantly from the beginning up to 0.2h in December 7–8 night, when the telescope was pointing towards Catania city, at variance with the steepening after 7.5h due to the Moon and Sun rise, when the ASTRI-Horn points better correlate with UVscope. On the other hand, the rapid variation in UVscope flux between 4.1h and 4.23h in the March 6–7 night, due to a cloud crossing its field of view, is not observed by ASTRI-Horn because within the errors.

The behaviour of ASTRI-Horn camera with respect to the NSB variations was better investigated with the correlation with UVscope measurements, as explained in the following section.

6.2 Correlation of the ASTRI-Horn and UVscope measurements

The temporal binning of the two instruments is very different: UVscope integrates the sky signals every second, while the ASTRI-Horn **PHDVAR** are averaged over ∼2 minutes. To correlate the two measurements, it was then necessary to average the UVscope flux over the ASTRI-Horn time intervals.

We plot the $PHDVAR$ as a function of the NSB flux measured by UVscope for the two considered observation nights. As an example, Fig. 7 shows the data relative to the 7–8 December night. We note that there are two remarkable behaviours: at low level of NSB flux, the $PHDVAR$s vary linearly with the NSB flux, while, at high fluxes, the $PHDVAR$s seem to reach a saturation level. The same behaviour is obtained in data relative to 6–7 March.

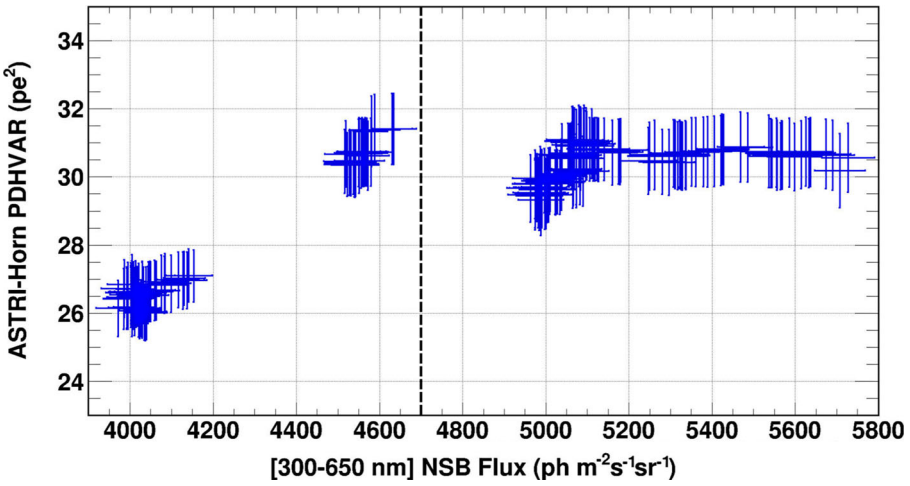

Fig. 7 ASTRI-Horn $PDHVAR$ – UVscope fluxes correlation for the 7-8 December 2018 night. The dashed black vertical line indicates the level we used to distinguish the linear regime from saturation

The level of NSB where the linear correlation transits to a constant is not well defined and, being correlated to the camera functioning, can be in principle different for each PDM. We then produced the correlations curves relative to each of the 9 PDMs and identify NSB_l=4700 ph m^{-2} ns^{-1} sr^{-1} (1.43 ph m^{-2} ns^{-1} deg^{-2}) as the flux value below which all PDMs are in a linear regime. Understanding this behaviour required ad-hoc studies with the use of simulations and laboratory measurements as discussed in the Section 7.2.

7 Discussion

The **PHDVAR** of the background fluctuation in the ASTRI-Horn camera derives from mainly two contributions and it can be computed from the statistical variance of the signal with the following formula:

$$PHDVAR = PHDVAR_{dark} + PHDVAR_{NSB} \tag{5}$$

where $\mathbf{PHDVAR_{dark}}$is the intrinsic standard deviation of the electronics plus the detector noise observed in dark condition, i.e. with closed lids and $\mathbf{PHDVAR_{NSB}}$ is the standard deviation induced by the NSB level that, being the signal Poissonian, is linearly correlated to the flux ($Flux_{NSB}$): $PHDVAR_{NSB} \propto Flux_{NSB}$. The correlation factor depends on several ingredients, as the two instrument working ranges, the ASTRI-Horn total efficiency (optics reflectivity plus filter transmission and SiPM photo-detection efficiency) and the camera electronics operation mode (i.e. the peak detector). Its value is not expected to vary unless one of the characteristics of the two systems changes. Moreover, if the NSB spectrum varies because of contamination from anthropic components or from Moon and Sun rise, variation of the correlation coefficient is also expected. We then expect that:

$$PHDVAR = PHDVAR_{dark} + A \times Flux_{NSB} \tag{6}$$

where A is the ASTRI-Horn variance – UVscope flux correlation factor.

The linear correlation between UVscope flux and ASTRI-Horn variance observed when the diffuse NSB flux is below ∼4700 ph m^{-2} ns^{-1} sr^{-1} (see Fig. 7), is then in agreement with Equation 6, while, above this flux, the camera outputs saturate. In the following section we present the analysis of the correlation splitting the discussion in two subsections, one for each regime.

7.1 Linear correlation regime

We analysed the linear regime in all observation nights listed in Table 1. In most of the cases it was not possible to constrain the value of A for different reasons: data below ∼4700 ph m^{-2} ns^{-1} sr^{-1} are too scarce, or no data at fluxes lower that NSB_l were present. The only two nights that present enough $PHDVAR$ data in the linear regime to give a statistically significant value for the slope A are 2018 December 7–8 and 2019 March 6–7, when the best fit values were $(7.89 \pm 0.45) \times 10^{-3}$ and $(6.10 \pm 0.39) \times 10^{-3}$, respectively. Figure 8 shows these data together with the relative best fitting lines.

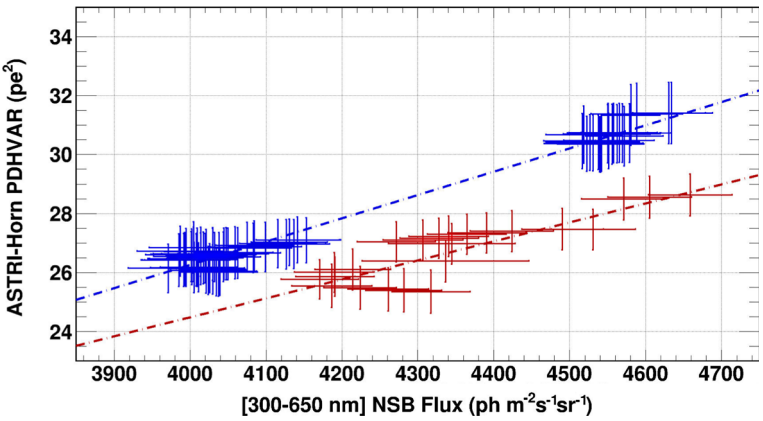

Fig. 8 ASTRI-Horn $PHDVAR$s as function of the UVscope fluxes for the 7-8 December 2018 (blue) and for the 6-7 March 2019 (red) night. The dash-dotted lines indicate the best fit models

The A values measured on December 2018 and on March 2019 are not compatible, being their ratio 0.77 ± 0.06. However, we know, from the results obtained with the muon ring analysis [9], that the telescope effective area measured in March 2019 was degraded by $\sim$25% after a strong Etna eruption in February 2019. The lower correlation slope can then be ascribed to the reduction of the optical throughput. This results makes the correlation between the ASTRI-Horn variance and the UV flux a good parameter for checking the stability of the telescope optical throughput together with other calibration methods (i.e. muon ring analysis, external calibrated light). The capability to observe variation of the optical throughput with $PHDVAR$ is limited by the statistics of the signal (6% in our data). In the upgraded version of ASTRI-Horn and in the ASTRI MA telescopes this error will be strongly reduced using $Variance$ data.

7.2 Saturation regime

The behaviour of the *PHDVAR*-NSB flux we observe above $\sim$4700 ph m^{-2} ns^{-1} sr^{-1} needed ad-hoc investigation in order to understand its origin. We compared the observed data with the results from a simulation of the ASTRI-Horn electronics and with laboratory measurements where we reproduced the level of NSB light present in Serra La Nave site, to check if a non linear response is expected from the SiPM plus electronics chain.

In the simulation, a given number of random UV photons depending of the NSB flux were used to generate the signal from the SiPM to be sent to the front-end electronics that shapes it with a 25 ns shaping time function and integrates all events falling in a 40 ns time window [13]. The resulting summed signal is then randomly sampled and the statistical distribution of these values is fitted with a Gaussian whose σ is correlated to the simulated level of NSB. As results, the simulated variances show a linear behaviour with the input flux, without any flattening.

Laboratory measurements were carried out, uniformly illuminating the PDM units with a continuous light, emulating the events generated by the NSB. The **RMS** of the output signal was measured and compared with the current produced inside the PDM. A linear response of the read-out electronics up to a average current value of $\sim$130 μA per pixel, corresponding to a NSB flux of $\sim$6500 ph m^{-2} ns^{-1} sr^{-1} (1.98 ph m^{-2} ns^{-1} deg^{-2}), is detected.

These two checks show that the SiPMs plus the read-out electronics present a linear behaviour with the NSB level without any pile-up, signal distortion or loss of information.

Further laboratory checks showed that the reason for the flattening of the $PHDVAR$, is a current consumption limit in the power system of all the camera pixels. The current limit for each PDM is $\sim$6 mA (corresponding to 4700 ph m^{-2} ns^{-1} sr^{-1}) and above this value the operative voltage of all sensors is reduced.

8 Conclusion

In this paper we investigated the correlation between the NSB fluxes measured by UVscope and ASTRI-Horn background variance $PHDVAR$ using contemporary data collected during the Crab Nebula observation campaign performed between December 2018 and March 2019. We found that only two sets of data were suitable for this analysis having long enough observation intervals with a NSB level lower than $\sim$4700 ph m^{-2} ns^{-1} sr^{-1} above which the camera response starts to saturate because of a limit in the power supply. We discovered that there is a linear correlation between the variance measured in the ASTRI-Horn camera pixels and the flux measured by UVscope, quantified through the slope A. This correlation that depends on several parameters is expected not to vary unless some of the two instruments characteristic changes. We detected a reduction of A of about 25% between the two data sets due to a degradation of the optics reflectivity. In this context, the presented analysis is a sort of preview of what would be possible to do with $Variance$. In fact, it suggests that the study of the correlation between the *Variance* measured by ASTRI-Horn telescopes and the NSB flux measured by UVscope is an useful diagnostic tool that can quickly point out reduction of the overall throughput. The measurement of the correlation A can be used to monitor the long term variation of the telescope optical throughput becoming complementary to other planned methods. It is clear that an external system is necessary to distinguish between NSB spectral variations and efficiency loss of the optical system and it is represented by UVscope in the case of ASTRI-Horn.

The limit in the PDM power system of ASTRI-Horn has been increased in the updated version of the camera to greatly alleviate the saturation problem. Considering that UVscope will continue to be operative during the future observation campaigns, the results presented in this paper could be consolidated with larger data set. Moreover, the saturation effect will not be present in the cameras designed for the ASTRI MA telescopes where an upgraded version of the power system will be able to supply a constant power up to 10 times the current level. At the same time, a new generation of UVscope, called UVSiPM, equipped with the same SiPM sensors of the ASTRI

camera, to entirely match the two spectral responses, is under design for its use in ASTRI MA.

Although in the ASTRI MA framework, the value of the parameter A is expected to be different with respect that measured by ASTRI-Horn, the analysis methods here presented and the conclusion we drew will be still applied to the forthcoming ASTRI MA.

Acknowledgements Authors thank the anonymous referee for his/her improving the clarity of the paper and Ciro Bigongiari for his insightful comments. This work was conducted in the context of the ASTRI Project, supported by the Italian Ministry of Education, University and Research (MIUR) with funds specifically assigned to the Italian National Institute of Astrophysics (INAF) and by the Italian Ministry of Economic Development (MISE) within the Astronomia Industriale program. This work has gone through internal review by the ASTRI Project Collaboration.

Data Availability The datasets analysed during the current study are not publicly available being taken during the commissioning phase of the telescope, but are available from the corresponding author on reasonable request.

Declarations

Conflict of Interests The authors declare that they have no conflicts of interest.

References

1. Catalano, O., Capalbi, M., Gargano, C., et al: The ASTRI camera for the Cherenkov Telescope Array. In: Society of Photo-Optical Instrumentation Engineers (SPIE) Conference Series, vol 10702, p 1070237. https://doi.org/10.1117/12.2314984 (2018)
2. Giro, E., Canestrari, R., Sironi, G., et al: First optical validation of a Schwarzschild Couder telescope: the ASTRI SST-2M Cherenkov telescope. 608:A86. https://doi.org/10.1051/0004-6361/201731602, arXiv:1709.08418 (2017)
3. d'Arturo, H.G.: The tessellated mirror. Journal of the British Astronomical Association **63**, 71–74 (1953)
4. Leinert, C., Bowyer, S., Haikala, L.K., et al.: The 1997 reference of diffuse night sky brightness. 127, pp 1–99. https://doi.org/10.1051/aas:1998105 (1998)
5. Lombardi, S., Catalano, O., Scuderi, S., et al: First detection of the Crab Nebula at TeV energies with a Cherenkov telescope in a dual-mirror Schwarzschild-Couder configuration: the ASTRI-Horn telescope. 634:A22. https://doi.org/10.1051/0004-6361/201936791, arXiv:1909.12149 (2020)
6. Maccarone, M.C., Catalano, O., Giarrusso, S., et al.: Performance and applications of the UVscope instrument. Nucl. Inst. Methods Phys. Res. A **659**, 569–578 (2011). https://doi.org/10.1016/j.nima.2011.08.004
7. Maccarone, M.C., Leto, G., Bruno, P., et al: The site of the ASTRI SST-2M telescope prototype. In: 33th International Cosmic Ray Conference (ICRC2013). arXiv:1307.5139 (2013)

8. Maccarone, M.C., La Rosa, G., Catalano, O., et al: UVscope and its application aboard the ASTRI-Horn telescope. Experimental Astronomy. https://doi.org/10.1007/s10686-021-09728-6, arXiv:2103.02233 (2021)
9. Mineo, T., Maccarone, M.C., Compagnino, A., et al: Muon calibration of the ASTRI-Horn telescope: preliminary results. In: 36th International Cosmic Ray Conference (ICRC2019), International Cosmic Ray Conference, vol 36, p 744, arXiv:1907.09197 (2019)
10. Ong, R.A.: Very high-energy gamma-ray astronomy. Physics Report **305**, 93–202 (1998). https://doi.org/10.1016/S0370-1573(98)00026-X
11. Rodeghiero, G., Catalano, O., Segreto, A., et al.: Illumination technique for the relative calibration of the ASTRI SST-2m camera. Nucl. Inst. Methods Phys. Res. A **764**, 176–185 (2014). https://doi.org/10.1016/j.nima.2014.07.038
12. Segreto, A., Catalano, O., Maccarone, M.C., et al: Calibration and monitoring of the ASTRI-Horn telescope by using the night-sky background measured by the photon-statistics ("variance") method. In: 36th International Cosmic Ray Conference (ICRC2019), International Cosmic Ray Conference, vol 36, p 791, arXiv:1909.08750 (2019)
13. Sottile, G., Catalano, O., La Rosa, G., et al: ASTRI SST-2M camera electronics. In: Hall, H.J., Gilmozzi, R., Marshall, H.K. (eds.) Ground-based and Airborne Telescopes VI, Society of Photo-Optical Instrumentation Engineers (SPIE) Conference Series, vol 9906, p 99063D https://doi.org/10.1117/12.2232464 (2016)